Heterosubstituted Diazonium Ions FNN^+, $HONN^+$, and H_2NNN^+. Automerization, Dediazoniation, and Deprotonation

Rainer Glaser* and Godwin Sik-Cheung Choy[1]

Department of Chemistry, University of Missouri—Columbia, Columbia, Missouri 65211
(Received: March 8, 1991)

Stationary structures on the potential energy surfaces of fluoro- (**1**), hydroxy- (**2**), and aminodiazonium ions (**3**) and of N_2O, HN_3, and CH_2N_2 were determined and characterized at the RHF/6-31G* and the MP2(full)/6-31G* levels, and reaction energies for automerization, dediazoniation, and deprotonation were determined up to full fourth order of Møller–Plesset theory with fully polarized triple valence basis sets. Geometries, IR spectra, relative isomer stabilities, and the activation energies for automerization are discussed. The stabilities of the diazonium ions with regard to dediazoniation and deprotonation were determined as well, and cation nitrogen affinities and proton affinities of the conjugated bases are reported. The electronegativity of the X group is used as the ordering principle, and effects of electron correlation are discussed throughout. The model dependency of relative energies and results of our prior higher level studies of methyldiazonium ion (**5**) and of available experimental structural, infrared, and energetic data suggest that this theoretical level is appropriate. At the correlated level, the ring structures of **1–3** are local minima and intermediates in the two-step automerizations of the more stable open structures. Electron correlation affects the potential energy surface of **1** drastically by changing the mode of automerization and that of **3** in a subtle but significant manner by changing the symmetry of the automerization pathway. Moreover, the C_{2v} symmetric open structure of **3** is found to be a transition-state structure for inversion of the most stable minimum of **3** with its pyramidal NH_2 group and overall C_s symmetry, suggesting that H_2N–N π-bonding is less important than had previously been thought. In general, increasing X electronegativity in XNN^+ stabilizes the open structures more than the bridged structures and the symmetrically bridged structures more than the asymmetrically bridged structures. Thus, relative isomer stabilities, activation energies for isomerization, and cation nitrogen affinities all increase with increasing X electronegativity. The proton affinities of N_2O, HN_3, and CH_2N_2 increase with decreasing X electronegativity; **2** is more acidic than **3** and **3** is more acidic than **5**. We found, surprisingly, that C_{2v} CH_2N_2 is not the minimum at the correlated level, but the inversion transition-state structure of C_s CH_2N_2 with its slightly pyramidalized CH_2 group and consequences are discussed. Basic concepts of orbital correlation, molecular graphs, and other topological properties show that the ring bonding is dominated by the a-symmetric interaction between X and N_2. Graphical analysis of the functions $\Delta\rho = \rho(\text{MP2}) - \rho(\text{RHF})$ show a general tendency of electron correlation to change T-shaped molecular graphs into ring graphs but not as the result of increased b-type interactions. This type of bonding together with MO theoretical perturbation analysis explains the unexpected stereochemistry of the ring-opening reaction.

Introduction

Unlike aromatic diazonium ions, aliphatic diazonium ions are highly reactive intermediates. Alkyldiazonium ions play an important role in various deamination reactions[2] that are pertinent to synthetic organic chemistry as well as to the understanding of the toxicological aspects of these reactions.[3] Yet, aliphatic diazonium ions have eluded a comprehensive characterization by physical organic techniques.[4] Our recent theoretical study of the bonding and the stability of a series of prototypical diazonium ions with C(sp^3), C(sp^2), and C(sp) carbon involvement in the CN linkages[5,6] revealed, surprisingly, that the commonly used Lewis structure for diazonium ions

$$X{-}N^+{\equiv}N$$

is inadequate. We proposed a new bonding model that is consistent with the electron density distributions in these ions. This model was subsequently shown to apply also to diazonium dication such as cyclopropeniumyldiazonium dications,[7] and it was confirmed with electron density analyses of correlated electron densities in a comparative study of methyl- and ethyldiazonium ions.[8] To further probe the nature of aliphatic diazonium ions, we have now studied the fluoro- (**1**), the hydroxy- (**2**), and the aminodiazonium ions (**3**). Here we report on the results of the potential surface analyses, and a study of the electronic structures will be presented elsewhere.[9]

Fluorodiazonium ion is well-known.[10] It can be prepared from *cis*-difluorodiazene and strong Lewis acid fluorides (SbF_5, AsF_5) to yield isolable salts. Moy and Young[11] first reported the preparation of $N_2F^+SbF_6^-$, and the structure was later confirmed by IR and Raman spectroscopies.[12-14] Hydroxydiazonium ion is still elusive.[15,16] Protonation of NO_2 in superacids did not result in a long-lived species, but there is evidence for the intermediacy of $HONN^+$ in the diazoniation of hydroxylamine with $NOBF_4$. Olah et al. succeeded in the preparation and spectroscopic characterization of the methoxydiazonium ion, CH_3ONN^+. This compound was found to be stable below −30 °C. At elevated temperatures these oxydiazonium ions were found to decompose with regeneration of N_2O. The existence of aminodiazonium ion was originally suggested by Schmidt,[17] and the first unequivocal formation and characterization of **2** were achieved by Olah's group by protonation of hydrazoic acid in superacids.[18] Spectroscopy

(1) (a) Presented in part at the 25th Midwest Regional Meeting of the American Chemical Society, Manhattan, KS, Nov 1990. (b) Part of the projected dissertation of Godwin Sik-Cheung Choy.
(2) Review: Kirmse, W. *Angew. Chem., Int. Ed. Engl.* **1976**, *415*, 251.
(3) For reviews see: Chapters 12–14 in *Chemical Carcinogens*; Vol. 2, ACS Monograph 182; Searle, Ch. E., Ed.; American Chemical Society: Washington, DC, 1984.
(4) Alkyldiazonium ions have been observed in superacid media, and methyldiazonium ion has been studied in the gas phase. In the solid state, alkyldiazonium ions can be stabilized in transition element complexes, but the alkyldiazonium ligands greatly differ from the free ions. See discussion in ref 5 and references therein.
(5) Glaser, R. *J. Phys. Chem.* **1989**, *93*, 7993.
(6) For recent theoretical work on aliphatic diazonium ions, see also: (a) Sapse, A.-M.; Allen, E. B.; Lown, J. W. *J. Am. Chem. Soc.* **1988**, *110*, 5671. (b) Ikuta, S. *J. Chem. Phys.* **1989**, *91*, 1376.
(7) Glaser, R. *J. Comput. Chem.* **1990**, *11*, 663.
(8) Glaser, R.; Choy, G. S.-C.; Hall, M. K. *J. Am. Chem. Soc.* **1991**, *113*, 1109.
(9) Glaser, R.; Choy, G. S.-C. Manuscript in preparation.
(10) Review on nonaromatic diazonium ions: Laali, K.; Olah, G. A. *Rev. Chem. Intermed.* **1985**, *6*, 237.
(11) Moy, D.; Young, A. R. *J. Am. Chem. Soc.* **1965**, *87*, 1889.
(12) Shamir, J.; Binenboym, J. *J. Mol. Struct.* **1969**, *4*, 98.
(13) Christe, K. O.; Wilson, R. D.; Sawodny, W. *J. Mol. Struct.* **1971**, *8*, 245.
(14) For N NMR studies of **1**, see: Mason, J.; Christe, K. O. *Inorg. Chem.* **1983**, *22*, 1849.
(15) **3** is more stable than its N-protonated isomer $HNNO^+$: Ferguson, E. F. *Chem. Phys. Lett.* **1989**, *156*, 319.
(16) Olah, G. A.; Herges, R.; Laali, K.; Segal, G. A. *J. Am. Chem. Soc.* **1986**, *108*, 2054.
(17) Schmidt, A. *Chem. Ber.* **1966**, *99*, 2976.

0022-3654/91/2095-7682$02.50/0

and theory showed that the aminodiazonium ion is favored over the iminodiazenium ion.

In this article, we discuss the potential energy surfaces of **1–3** in comparison to alkyldiazonium ion. Minima and transition-state structures along the automerization pathway have been determined both at the restricted Hartree–Fock level and with the inclusion of perturbational corrections for electron correlation. Significant qualitative and quantitative differences were found. We then discuss the geometries and IR spectra, the relative stabilities between the open and the symmetrically bridged structures, the stereochemistry of the automerization pathway, and its electronic origin, report on the thermodynamic stabilities with regard to automerization, and compare the dediazoniation reactions via the nitrogen affinities. N_2O, HN_3, and diazomethane have also been considered, and their proton affinities are reported. Diazomethane was found to deviate from C_{2v} symmetry at the correlated level, and consequences are discussed. Effects of electron correlation on the various aspects are discussed, and dependence on electronegativity is used as the ordering principle.[19]

Computational Methods

Geometry optimizations were performed under the constraints of the symmetry point groups specified with the gradient algorithm of Schlegel using GAUSSIAN88.[20] The exact Hessian matrix was then computed at the RHF and at the MP2 levels for each of the structures to assure the stationarity of the located extrema, to characterize these extrema as minima and transition-state structures via the number of negative eigenvalues, and to determine the harmonic vibrational frequencies together with their IR intensities and the vibrational zero-point energies (VZPEs). Frequencies and VZPEs always are given as calculated. The respective RHF values require scaling by the usual factor[21] of 0.9 while the MP2 derived values were used unscaled. The program SPECTRUM[22] was used to display the calculated IR spectra in graphical form.

In general, structural optimizations and the normal-mode analyses were carried out at the restricted Hartree–Fock (RHF) level and subsequently with the inclusion of the perturbational effects of electron correlation at the second-order Møller–Plesset[23] level with the 6-31G* basis set,[24] MP2(full)/6-31G*. Higher order Møller–Plesset perturbation theory was used to determine more reliable energies. Energy computations were carried out at the full fourth-order level of Møller–Plesset perturbation theory in the frozen core approximation with the valence triple-ζ basis set[25] 6-311G** using both the RHF/6-31G* and the MP2(full)/6-31G* optimized structures. Surface and contour plots of the electron densities of the ring structures were computed with the program NETZ,[26] displayed with our PV wave programs, and analyzed topologically with Bader's EXTREME.[27] The correlated electron densities were calculated with Frisch's implementation of the Z-vector method.[28]

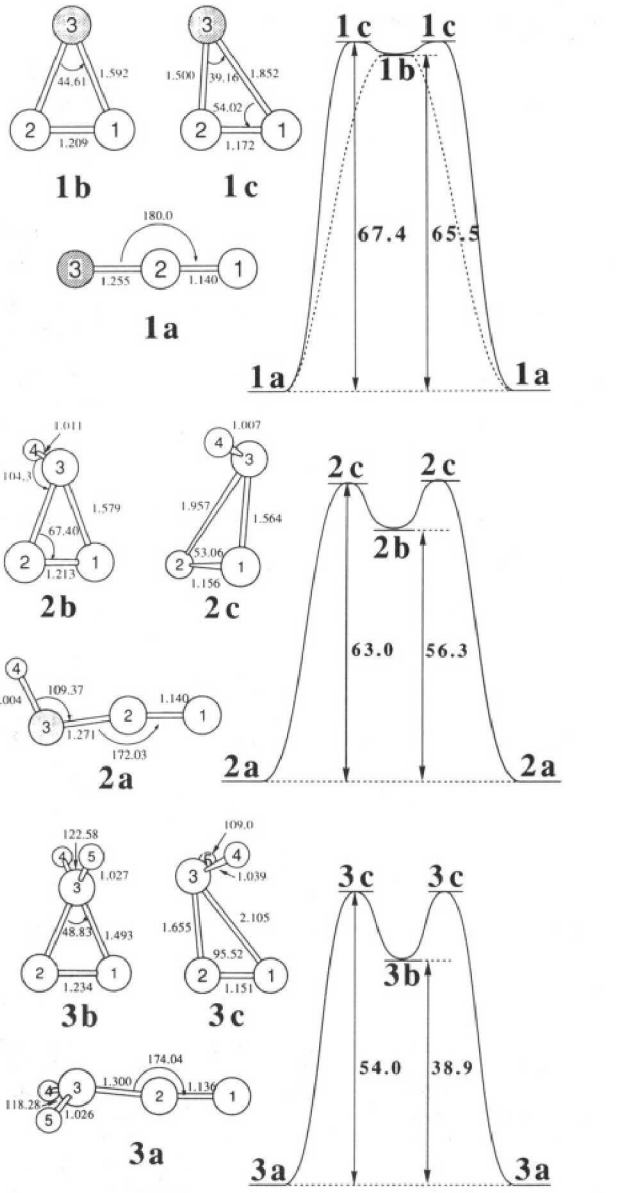

Figure 1. Reaction coordinates for the automerization processes of fluorodiazonium ion (**1**, top), hydroxydiazonium ion (**2**, center), and aminodiazonium ion (**3**, bottom). The MP2(full)/6-31G* optimized geometries are displayed. Energies are those determined at MP4-[SDTQ]/-6-311G**//MP2(full)/6-31G*, and the potential energy surfaces are drawn to scale. The dashed line schematically shows the reaction coordinate for the automerization mechanism of the fluorodiazonium ion at the RHF level.

Computations were carried out on a Vaxstation3100, a Vaxstation3520, a network of Silicon Graphics Personal Iris workstations and servers, and on the IBM 4381 and 3090 mainframes of the Campus Computing Center and the attached FPS array processor.

Results and Discussion

The potential energy surfaces of **1–3** were searched for stationary structures at the RHF/6-31G* and MP2(full)/6-31G* levels. We have previously reported the corresponding studies of methyldiazonium ion.[29] The open structures were optimized either

(18) Mertens, A.; Lammertsma, K.; Arvanaghi, M.; Olah, G. A. *J. Am. Chem. Soc.* **1983**, *105*, 5657.

(19) For group electronegativities used here, see: Wells, P. R. *Prog. Phys. Org. Chem.* **1968**, *6*, 111. They are 3.95 (F), 3.70 (OH), 3.35 (NH_2), and 2.30 (CH_3). Slightly different numerical values are without consequence for our discussion as we use electronegativity merely as an ordering principle.

(20) Frisch, M. J.; Head-Gordon, M.; Schlegel, H. B.; Raghavachari, K.; Binkley, J. S.; Gonzales, C.; Defrees, D. J.; Fox, D. J.; Whiteside, R. A.; Seeger, R.; Melius, C. F.; Baker, J.; Martin, R. L.; Kahn, L. R.; Stewart, J. J. P.; Fluder, E. M.; Topiol, S.; Pople, J. A. *GAUSSIAN88 (Rev. C)*; Gaussian, Inc.: Pittsburgh, PA, 1988.

(21) Hehre, W. J.; Radom, L.; Schleyer, P. v. R.; Pople, J. A. *Ab Initio Molecular Orbital Theory*; John Wiley & Sons: New York, 1986.

(22) Spectrum: Hall, M. K.; Glaser, R. Department of Chemistry, University of Missouri—Columbia, 1990.

(23) (a) Møller, C.; Plesset, M. S. *Phys. Rev.* **1934**, *46*, 1243. (b) Binkley, J. S.; Pople, J. A. *Int. J. Quantum Chem.* **1975**, *9*, 229. (c) Pople, J. A.; Seeger, R. *Int. J. Quantum Chem.* **1976**, *10*, 1. (d) Pople, J. A.; Krishnan, R.; Schlegel, H. B.; Binkley, J. S. *Int. J. Quantum Chem.* **1978**, *14*, 91.

(24) (a) Hehre, W. J.; Ditchfield, R.; Pople, J. A. *J. Chem. Phys.* **1972**, *56*, 2257. (b) Hariharan, P. C.; Pople, J. A. *Theor. Chim. Acta* **1973**, *28*, 213. (c) Binkley, J. S.; Gordon, M. S.; DeFress, D. J.; Pople, J. A. *J. Chem. Phys.* **1982**, *77*, 3654. (d) Six Cartesian second-order Gaussians were used for d shells.

(25) (a) Krishnan, R.; Binkley, J. S.; Seeger, R.; Pople, J. A. *J. Chem. Phys.* **1980**, *72*, 650. (b) Five pure d orbitals were used in conjunction with the valence-triple-ζ basis sets.

(26) Glaser, R. Department of Chemistry, University of Missouri—Columbia, 1990.

(27) (a) Biegler-Koenig, F. W.; Bader, R. F. W.; Tang, T. H. *J. Comput. Chem.* **1982**, *3*, 317. (b) This program was ported both to the IBM 4381 by G. Choy and to the Silicon Graphics Personal Iris by R. Glaser.

(28) (a) Handy, N. C.; Schaefer III, H. F. *J. Chem. Phys.* **1984**, *81*, 5031. (b) Reference 20.

TABLE I: Total, Relative, and Vibrational Zero-Point Energies[a-d]

	RHF/6-31G*				MP2/6-31G*		/6-311G**//RHF/6-31G*	
		VZPE	RHF/6-31G*	RHF/6-311G**	VZPE	MP2/6-31G*	MP2	MP3
1a	M	7.16	207.831 027	207.886 563	M 5.86	208.333 586	208.418 711	208.407 357
1b	TS	4.35	207.728 576	207.774 223	M 4.39	208.227 250	208.322 789	208.300 328
			(64.29)	(70.49)		(66.73)	(60.19)	(67.16)
1c					TS 3.94	208.218 754		
						(72.06)		
2a	M	14.56	183.916 215	183.971 612	M 12.79	184.423 874	184.497 472	184.488 683
2b	M	12.79	183.822 989	183.873 713	M 12.40	184.331 420	184.395 982	184.397 479
			(58.50)	(61.43)		(58.02)	(63.69)	(57.23)
2c	TS	12.25	183.822 187	183.873 063	TS 11.41	184.313 830	184.388 936	184.389 055
			(59.00)	(61.84)		(69.05)	(68.11)	(62.52)
3a	M	23.10	164.153 431	164.202 412	M 21.32	164.643 299	164.706 365	164.704 534
3b	M	23.63	164.085 574	164.133 158	M 21.51	164.578 795	164.640 452	164.645 875
			(42.58)	(43.46)		(40.48)	(41.36)	(36.81)
3c[e]	TS	21.44	164.072 135	164.119 552	SS 19.22	164.546 752	164.617 661	164.622 246
			(51.01)	(52.00)		(60.58)	(55.66)	(51.64)
					TS 19.39	164.547 472		
						(60.13)		
3d	TS	22.36	164.152 080	164.200 991	M 20.80	164.642 245	164.705 637	164.703 368
			(0.85)	(0.89)		(0.66)	(0.46)	(0.73)
4a	M	12.11	146.875 079 2	146.912 175	M	147.292 357	147.334 223	147.341 783
4b	M	14.52	146.907 399	146.941 600	M	147.329 888	147.368 193	147.376 018
			(−20.28)	(−18.46)		(−23.55)	(−21.32)	(−21.48)
4c	TS	11.56	146.817 302	146.854 423	TS	147.240 326	147.286 764	147.294 623
			(36.26)	(36.24)		(32.65)	(29.78)	(29.59)
F^+			98.632 610	98.659 470		98.730 384	98.791 712	98.809 098
			(159.68)	(160.25)		(214.37)	(209.78)	(195.69)
OH^+		4.83	74.830 216	74.858 478		74.947 024	74.995 041	75.013 305
			(89.12)	(88.74)		(135.09)	(131.61)	(118.58)
H_2N^+		12.36	55.127 291	55.149 351		55.244 187	55.278 722	55.298 036
			(51.58)	(51.04)		(86.31)	(84.68)	(75.36)
N_2O	M	7.73	183.680 122	183.727 814	M 6.74	184.213 684	184.273 439	184.246 710
			(148.15)	(152.99)		(131.90)	(140.58)	(151.84)
HN_3	M	14.56	163.838 696	163.882 595	M 13.51	164.351 248	164.406 673	164.391 837
			(197.50)	(200.69)		(183.26)	(188.06)	(196.22)
CH_2N_2	M	21.59	147.843 784	147.881 711	TS 19.90	148.310 594	147.881 711	148.367 229
			(233.60)	(234.91)		(223.10)	(222.86)	(227.10)
					M 20.06	148.310 598		
N_2		3.94	108.943 949	108.971 717		109.261 574	109.292 698	109.286 408

[a] Vibrational zero-point energies (VZPE) are given in kilocalories per mole as computed at the RHF/6-31G* level. M indicates a minimum and TS denotes a transition-state structure. [b] Total energies (−*E*) are given in atomic units. Values given in parentheses for **1**–**4** are relative energies in kilocalories per mole with regard to the respective most stable stationary structure, and values given in parentheses for N_2O, HN_3, and CH_2N_2 are their proton affinities. [c] Reaction energies in kilocalories per mole for the association reactions of X^+ with N_2 are given in parentheses below the total energies of the cations X^+. [d] All electrons were correlated at the MP2/6-31G* level. MP*x* energies at the levels MP*x*/6-311G** were calculated with the frozen core approximation and based on the RHF/6-31G* and MP2(full)/6-31G* geometries. [e] The first row of data for **3c** refers to the C_s symmetric structure; this structure is a transition-state structure (TS) at the RHF level but a second-order saddle point structure (SS) at the correlated level. The second entry at the correlated level refers to the chiral transition-state structure.

in C_s symmetry (X = OH, NH_2) or with imposed linearity (X = F), and the structures thus obtained are referred to as the a-isomers. The bridged geometries, denoted as b-structures, were optimized either in C_s symmetry (X = OH, NH_2) or in C_{2v} symmetry (X = F). If both of these types of topologies corresponded to (local) minima, then the transition-state structure for isomerization was located as well and their geometries are referred to as the c-structures. Energies were computed up to full fourth order of Møller–Plesset perturbation theory with the 6-311G** basis set based on the geometries localized at RHF/6-31G* and at MP2(full)/6-31G*. In Table I, the total energies and the vibrational zero-point energies determined at the two levels of optimization are listed together with the characters of the stationary structures. Geometrical parameters are compiled in Table II. The products of deprotonation, N_2O, HN_3, and CH_2N_2, were studied in the same fashion, and their energies are included in Table I and geometries are given in Table III. Frequencies and IR intensities are given for all molecules in Table IV.

Correlation Effects on the Automerization Pathways. The a-type structures are the most stable ones for **1**–**3**. All of the b-type structures of **1**–**3** are found to be local minima at the MP2-(full)/6-31G* level; that is, the automerizations are two-step processes in all cases via a bridged intermediate. Molecular model type drawings of these structures are shown in Figure 1 together with the schematically (but to scale) drawn energy profiles for the pathways for automerization of the a-type diazonium ions via the bridged c-type transition-state structures and the symmetrically bridged b-type intermediates. The activation energies given in these figures are those determined at our highest level, MP4-[STDQ]/6-311G**//MP2/6-31G*. Electron correlation affects the potential energy surfaces of **1** and **3** in a *qualitative* manner, whereas the potential energy surface of **2** exhibits only quantitative differences. These differences are discussed first, and the energetic and structural aspects are discussed subsequently.

Fluorodiazonium Ion. On the RHF/6-31G* potential energy surface, **1b** is not a local minimum but it is the transition-state structure for the automerization reaction as indicated by the dashed line in Figure 1. Suppose we had made use of the frequently employed (and common accepted) procedure of exploring the potential energy surface at the RHF level only and to then calculate "better" relative energies at the correlated level. We would find that the higher level energies MP*x*(fc)/6-311G**//RHF/6-31G* give rather similar relative energies for **1a** and **1b** (Table I). We would then be inclined to deduct (erroneously) that the automerization of **1** remains a *one-step* process even at the correlated level and that the activation barrier changes little. For example, if one compares the relative energies between **1a** and **1b** determined at RHF/6-31G* with those determined at

(29) See refs 5 and 8 for computations of $CH_3N_2^+$ based on the RHF and on the MP2 structures.

TABLE I (continued)

/6-311G**//RHF/6-31G*			/6-311G**//MP2(full)/6-31G*				
MP4[DQ]	MP4[SDQ]	MP4[SDTQ]	MP2	MP3	MP4[DQ]	MP4[SDQ]	MP4[SDTQ]
208.412 242	208.421 968	208.447 897	208.426 089 7	208.403 925	208.412 016	208.424 294	208.455 864
108.302 604	208.313 880	208.343 454	208.308 282	208.299 716	208.302 843	208.316 961	208.351 440
(68.80)	(67.83)	(65.54)	(73.93)	(65.41)	(68.51)	(67.35)	(65.53)
			208.303 033	208.301 094	208.304 954	208.318 460	208.348 492
			(77.22)	(64.54)	(67.18)	(66.41)	(67.38)
184.493 433	184.502 192	184.528 706	184.504 679	184.485 227	184.492 939	184.504 051	184.536 077
184.397 130	184.406 737	184.436 246	184.406 305	184.396 533	184.399 834	184.411 824	184.446 351
(60.43)	(59.90)	(58.02)	(61.73)	(55.66)	(58.42)	(57.87)	(56.30)
184.391 951	184.401 916	184.430 984	184.390 889	184.387 677	184.392 344	184.404 566	184.435 673
(63.68)	(62.92)	(61.32)	(71.40)	(61.21)	(63.12)	(62.43)	(63.00)
164.708 976	164.716 328	164.741 353	164.712 710	164.702 741	164.709 273	164.718 554	164.747 930
164.647 175	164.653 534	164.678 817	164.646 944	164.646 603	164.648 715	164.656 533	164.685 873
(38.78)	(39.40)	(39.24)	(41.27)	(35.23)	(38.00)	(38.92)	(38.94)
164.624 825	164.632 203	164.659 082	164.617 128	164.614 811	164.621 357	164.631 514	164.661 814
(52.81)	(52.79)	(51.63)	(59.98)	(55.18)	(55.17)	(54.62)	(54.04)
			164.617 092	164.614 800	164.621 256	164.631 403	164.661 761
			(59.66)	(55.18)	(55.23)	(54.69)	(50.04)
164.707 514	164.714 909	164.740 004	164.711 275	164.701 974	164.707 966	164.717 275	164.746 343
(0.92)	(0.89)	(0.85)	(0.90)	(0.48)	(0.82)	(0.80)	(1.00)
147.348 713	147.355 543	147.377 244	147.340 204	147.341 112	147.348 886	147.357 963	147.383 983
147.376 609	147.381 894	147.405 288	147.373 820	147.377 421	147.378 348	147.384 882	147.412 130
(−17.51)	(−16.54)	(−17.60)	(−21.09)	(−22.18)	(−18.49)	(−16.89)	(−17.66)
147.297 963	147.304 925	147.330 492					
(31.85)	(31.76)	(29.34)					
98.813 396	98.813 726	98.814 949	98.791 712	98.809 098	98.813 396	98.813 726	98.814 949
(193.26)	(196.00)	(202.22)	(211.85)	(195.20)	(193.38)	(196.9)	(203.79)
75.016 970	75.017 561	75.019 405	74.994 956	75.013 245	75.016 913	75.017 532	75.019 415
(116.46)	(118.43)	(123.63)	(133.62)	(118.10)	(116.46)	(119.06)	(125.85)
55.301 424	55.301 930	55.303 907	55.279 333	55.298 792	55.302 214	55.302 753	55.304 792
(73.22)	(74.36)	(78.54)	(85.72)	(75.41)	(73.18)	(74.68)	(79.68)
184.252 142	184.265 415	184.301 360	184.282 832	184.241 180	184.250 249	184.266 939	184.311 966
(151.41)	(148.58)	(142.66)	(139.21)	(153.14)	(152.29)	(148.79)	(140.63)
164.395 395	164.405 708	164.327 565	164.413 012	164.389 973	164.395 362	164.408 054	164.446 087
(196.78)	(194.92)	(190.10)	(188.06)	(196.27)	(196.98)	(194.84)	(189.41)
148.367 883	148.378 581	148.404 850	148.369 879	148.368 115	148.371 283	148.380 639	148.408 960
(230.64)	(227.82)	(224.94)	(225.07)	(225.38)	(228.87)	(227.77)	(225.94)
			148.369 908	148.368 012	148.371 194	148.380 553	148.408 951
109.290 866	109.295 896	109.312 285	109.296 780	109.283 782	109.290 442	109.296 785	109.316 155

MP4[SDTQ]/6-311G**//RHF/6-31G*, one finds a change in the relative energy that is smaller than 1.2 kcal/mol. Indeed, this close correspondence might be taken as an indication that the RHF approximation of the potential energy surface is quite sufficient. However, since we did explore the potential energy surface at the correlated level and with inclusion of the vibrational frequency analysis at that level, we do know that **1b** is in fact an intermediate along the *two-step* automerization. In other words, the c-type structures are not irrelevant for the automerization, and the activation energies for the automerization are determined by the relative energy between the a-type and the c-type structures. The important conclusion is then that erroneous deductions regarding the mode of automerization and its associated activation barriers would result because *the pathway from the a-type structure to the b-type structure is qualitatively changed when the electron correlation is taken into account.*

Aminodiazonium Ion. A more subtle but significant qualitative difference has been found for the automerization pathway of **3**. At the RHF level, **3c** was optimized in C_s symmetry, and the computation of the vibrational frequencies showed this structure to be the transition state; **3c** exhibited one imaginary frequency (i529.2 cm^{-1}, a′) with the expected displacement vector. Reoptimization and characterization of **3c** within the same symmetry at the MP2(full) level, however, showed this C_s symmetric structure to be a second-order saddle point. Aside from the imaginary mode (i485.5 cm^{-1}, a′) that corresponds to the in-plane displacement of the amino group toward either of the associated minima, a second low-frequency imaginary mode (i96.8 cm^{-1}, a″) occurred, and its displacement vector identified this mode as the amino torsion. Reoptimization without any symmetry constraints resulted in a chiral structure **3c**, which was shown to be the transition-state structure (i477.5 cm^{-1}, torsional mode is now positive with ν = 132.7 cm^{-1}) for automerization. The chiral structure **3c** and the corresponding second-order saddle point structure are structurally essentially the same except that the amino group is rotated in the transition state. The dihedral angles between the amino hydrogens and the plane of the nitrogens (see Table II) are 71.3° and −43.2°, and the amino group as a whole has thus been twisted by about 28.1°. At the MP2(full)/6-31G* level, the chiral structure is 0.45 and 0.28 kcal/mol more stable than the second-order saddle point without and with inclusion of the vibrational zero-point energies, respectively. Thus, on the MP2 potential energy surface there are two enantiomerically related pathways for the automerization process, while there is only one automerization pathway on the RHF surface along which the C_s symmetry is maintained. The situation is schematically displayed in Figure 2.

The open form of the aminodiazonium ion, **3a**, is characterized by a pyramidal amino group and an NNN angle of 174° (Figure 1). In **3b**, the N1–N2–N3 angle is reduced to 65° and the amino hydrogens are in one of the σ_v planes. Obviously, the reaction coordinate for the interconversion of **3b** to **3a** involves major changes both in the degree of the NH_2 pyramidalization and in the NNN angle. The transition-state structure shows (Figure 1) that NH_2 pyramidalization occurs first and that the NNN angle change occurs later along the reaction coordinate for automerization. Consequently, the $N2_s$ lone pair present in **3b** is essentially preserved in **3c**. Thus, these structural features suggest the

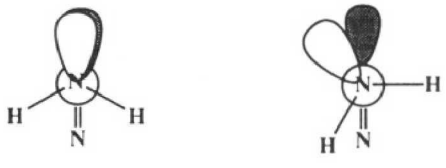

reduction of lone-pair repulsion as a likely and reasonable cause

TABLE II: Geometries of Diazonium Ions

parameter	a-structures RHF	a-structures MP2	b-structures RHF	b-structures MP2	c-structures RHF	c-structures MP2
			$(FNN)^+$			
N2-F3	1.240	1.255	1.583	1.592		1.501
N1-N2	1.072	1.140	1.136	1.209		1.172
N1-N2-F3	180.00	180.00	68.97	67.69		86.82
N1-F3-N2			42.07	44.61		
			$(HONN)^+$			
O3-H4	0.974	1.004	0.978	1.011	0.979	1.007
N2-O3	1.269	1.271	1.639	1.579	1.603	1.564
N1-N2	1.075	1.140	1.123	1.213	1.116	1.156
N2-O3-H4	109.33	109.37	103.22	104.30	100.27	100.07
N1-N2-O3	173.73	172.04	69.96	67.40	81.43	90.74
N1-O3-N2			40.08	45.19		
H4-O3-N2-N1	178.90	180.00	94.92	96.09	100.69	100.71
			$(H_2NNN)^+$			
N3-H4	1.007	1.026	1.007	1.027	1.010	1.039
N3-H5						1.038
N1-N2	1.078	1.136	1.160	1.234	1.116	1.151
N2-N3	1.308	1.300	1.466	1.493	1.711	1.655
H4-N3-N2	112.10	113.47	116.54	115.94	96.10	106.23
H5-N3-N2						102.98
N1-N2-N3	175.10	174.04	66.70	65.58	68.98	95.52
H5-N3-H4	117.98	118.28	121.79	112.59	118.11	109.00
N2-N3-N1			46.59	48.83		32.97
H4-N3-N2-N1	112.30	110.99	102.42	102.75	120.40	-43.20
H5-N3-N2-N1						71.32
			$(HCNN)^+$			
N1-N2	1.081	1.138	1.286	1.357	1.127	1.157
N2-C3	1.484	1.434	1.297	1.335	1.702	2.110
C3-H4	1.090	1.105	1.078	1.090	1.092	1.122
N1-N2-C3	167.76	162.33	60.27	59.44	64.80	57.19
N2-C3-H4	102.50	105.13	150.27	149.45	86.28	73.09
N1-C3-N2			59.46	61.12		
H-C-N-N	180.00	180.00	180.00	180.00		

[a] In angstroms and degrees. [b] The structure of the second-order saddle point of **3c** obtained at MP2(full)/6-31G* is as follows: N3-H4, 1.038; N1-N2, 1.150; N2-N3, 1.658; H5-N3-N2, 104.47; N1-N2-N3, 96.17; H5-N3-N2-N1, 57.19.

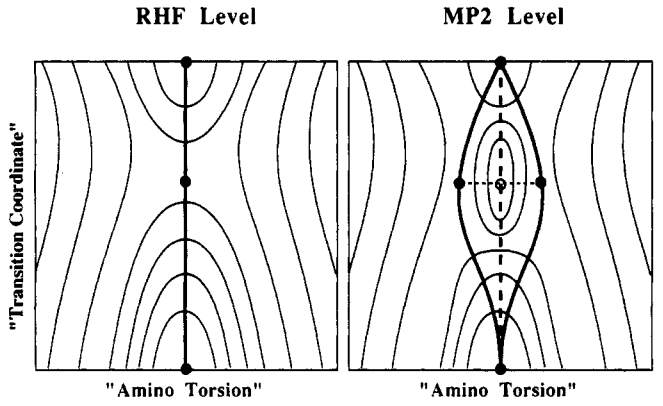

Figure 2. Schematic drawings of the RHF (left) and MP2(full)/6-31G* potential energy surfaces of aminodiazonium ion. The potential energy surfaces are shown as a function of the transition coordinate—an unspecified combination of NH_2 pyramidalization and NNN angle variation—and the amino torsion coordinate. At the RHF level, C_s symmetry is maintained along the automerization pathway, while the isomerization involves a pair of enantiomerically related pathways on the MP2 surface.

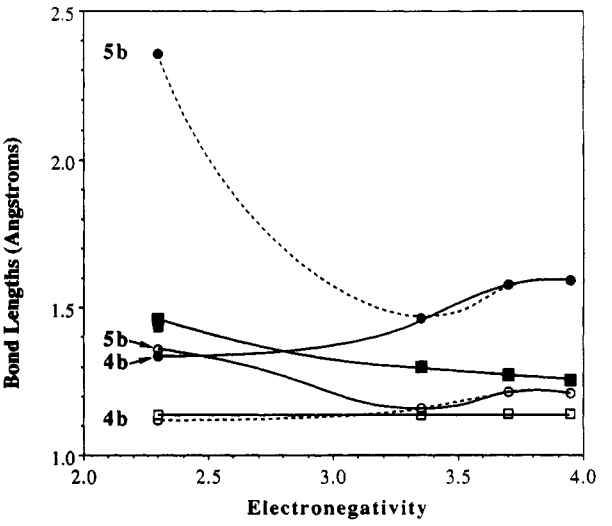

Figure 3. Changes of the NN (unfilled) and the XN (solid) bond lengths are shown as a function of the X group electronegativity for the a-type structures (squares) and for the bridged b-type structures (circles). Solid lines of interpolation are drawn for the molecules **1–3** and methyldiazonium cation (**5**). The dashed interpolation curves result when the data for model compound **4** are used instead of those of **5**.

for the deviation from C_s symmetry along the automerization pathway. Newman projections illustrate the point nicely.

Structures and Infrared Spectra. *Geometries.* The MP2-(full)/6-31G* geometries of **1–3** are discussed in comparison to carbenediazonium ion (**4**, a model system whose purpose will be discussed below) and methyldiazonium ion, **5**. The identity of the X group in the open isomers of all of the diazonium ions leaves the NN bond length essentially unaffected. The NN bond lengths are confined to the very narrow range of 1.136–1.140 Å for **1–4** (see Figure 3)—slightly longer than the bond in N_2—and the NN bond in **5** is slightly shorter (1.128 Å). More variation is found for the NN bonds in the symmetrically bridged structures; they are generally longer, and they increase with decreasing electronegativity of the X group. Methyldiazonium ion stands out in this regard as **5b** essentially is not bonded at all, but the model system **4b** fits the trend. The XN bond lengths show the expected decrease with *increasing* electronegativity of X in the open isomers, while the XN bond lengths in the b-type structures are significantly

TABLE III: Geometries of N_2O, HN_3, and CH_2N_2[a-d]

	N_2O			HN_3			CH_2N_2 (C_{2v})		
	RHF	MP2	expt	RHF	MP2	expt	RHF	MP2	expt
N2-N1	1.092	1.171	1.128	1.0989	1.158	1.134	1.116	1.150	1.139
Δ(N-N)	-0.036	+0.043		-0.036	+0.024		-0.023	+0.012	
X-N2	1.179	1.192	1.184	1.239	1.250	1.243	1.280	1.310	1.300
Δ(X-N)	-0.005	+0.008		-0.004	+0.007		-0.020	+0.010	
H-X				1.006	1.023	1.015	1.068	1.077	1.075
X-N2-N1				173.8[e]	171.1[e]	171.3[e]			
H-X-N				108.3	110.4	108.8	117.8	117.3	117.0

[a] In angstroms and degrees. Δ(N-N) and Δ(X-N) are the differences with regard to the experimental values. [b] RHF geometries from ref 35. [c] Experimental geometries. N_2O: Burris, G. A.; Gordy, W. *Phys. Rev.* **1956**, *101*, 599. HN_3: Winnewisser, B. P. *J. Mol. Spectrosc.* **1980**, *82*, 220. CH_2N_2: Cox, A. P.; Thomas, L. F.; Sheridan, J. *Nature* **1950**, *181*, 1000. [d] The C_s symmetric structure of CH_2N_2 obtained at the MP2(full)/6-31G* level: CN, 1.3106; NN, 1.1498; CH, 1.0773; NNC, 178.8348 (transoid); HCN, 117.0229; HCNX, 94.9437. [e] Transoid.

TABLE IV: Vibrational Spectra[a]

description and mode symmetry	MP2(full) ν	MP2(full) int	expt ν	expt ν
	FNN^+			
NN stretch, σ_g	2173	17	2370[b]	2371[c]
FN stretch, σ_g	1083	54	1056	1057
FNN deformation, π	421	2	803	391
	$HONN^+$			
OH stretch, a′	3398	498		
NN stretch, a′	2199	30		
H bending, a′	1359	138		
ON stretch, a′	1096	84		
ONN deformation, a″	461	5		
ONN deformation, a′	434	16		
	H_2NNN^+			
NH stretch, a″	3568	380		
NH stretch, a′	3435	302		
NN stretch	2335	42		
HNH bending, a′	1640	101		
NH_2 rocking, a″	1315	0		
NN stretch, a′	1146	12		
umbrella, a′	581	356		
NNN deformation, a′	469	11		
NNN deformation, a″	424	2		
	ONN			
*NN*O stretch, σ_g	2257	264	2224[d]	
N*NO* stretch, σ_g	1293	8	1285	
NNO deformation, π	584	5	589	
	HN_3			
NH stretch, a′	3521	67		
N*NN*H stretch, a′	2396	198		
NNN stretch, a′	1271	1		
HNN deformation, a′	1129	222		
NNN deformation, a″	580	1		
NNN deformation, a′	553	27		
	CH_2N_2			
CH asym stretch, b_2	3414	4		3411[f]
CH sym stretch, a_1	3279	27	3077[e]	3276
NN stretch, a_1	2410	249	2102	2410
CH_2 bending, a_1	1467	21	1414	1467
CN stretch, a_1	1188	3	1170	1186
deformation, b_2	1139	1	564	1140
CNN deformation, b_1	573	1	421	573
CNN deformation, b_2	450	1	406	450
CH_2 "pyramidalization", b_1	-94	178		113

[a] MP2(full)/6-31G* frequencies are given in wavenumbers and IR intensities are given in km/mol. Mole descriptions are approximate. [b] Reference 12. [c] Reference 13. [d] Herzberg, G. *Molecular Spectra and Molecular Structure III. Electronic Spectra and Electronic Structure of Polyatomic Molecules*; Van Nostrand Reinhold: New York, 1966; p 596. [e] Moore, C. B.; Pimentel, G. C. *J. Chem. Phys.* **1964**, *40*, 329. [f] MP2(full)/6-31G* frequencies of C_s diazomethane.

longer and decrease with *decreasing* electronegativity of X (Figure 3).

An interesting feature in the open isomers relates to the small deviation of the XNN backbone from linearity in **2a** and **3a**. This nonlinearity was previously found for **2a** at the 4-31G level by Olah et al.,[16] but in their study the hydroxy H and the terminal N were in a cisoid relation instead of the transoid relation as found in our work.

Another difference relates to the overall symmetry of **3a**. Mertens et al.[18] had previously studied **3** at the RHF/3-21G level and found the structure to be C_{2v} symmetric. We find that the most stable minimum of **3** is actually pyramidal at the amino N, **3a**, and that the C_{2v} symmetric structure, **3d**, is the transition-state structure for NH_2 inversion in **3a**. The C_{2v} structure **3d** was

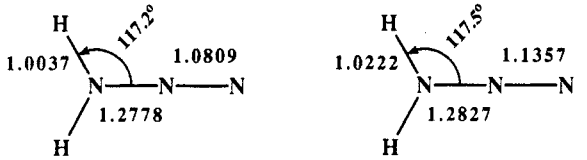

RHF/6-31G* **3d** MP2(full)/6-31G*

optimized and characterized at both the RHF/6-31G* and the MP2(full)/6-31G* levels, and one imaginary frequency (b_1, RHF: *i*433 cm^{-1}; MP2: *i*407 cm^{-1}) was found at each level. The activation barriers determined at the various levels vary between 0.5 and 1 kcal/mol. At the levels of optimization and at our highest level the activation energies are 0.85 (RHF), 0.66 (MP2), and 1.00 kcal/mol, and the inclusion of vibrational zero-point energy corrections results in the corresponding values of 0.18, 0.14, and 0.48 kcal/mol. Although the barrier is small, the finding that the open structure of **3** prefers a pyramidal amino group and not a planar one is rather significant with regard to the implications on the H_2N-N_2 bonding. Mertens et al.[18] concluded that the H_2N-N bond had significant double-bond character based on the planarity of the molecule and the short H_2N-N bond length. Our results suggest that *the H_2N-N π-bond is much less important than had previously been thought* and implies that other factors have to be responsible for the remarkably short bond length. We are in the process of analyzing this interesting bonding feature with electron density analysis techniques to determine its electronic origin.[9]

Vibrational Spectra. The IR spectra of **1a-3a** have been determined at the correlated level, and they are shown in Figure 4. The spectrum of **1a** is especially important since the infrared and Raman spectra of the FNN^+ cation are known for the hexafluoroantimonate salt (Table IV). The agreement between the experimental and our theoretical spectra is excellent for the FN stretching mode as well as for the bending mode, adding credence to our choice of the theoretical level. These results confirm the reassignment[13] of the deformational mode of **1a** to 390 cm^{-1} as opposed to its earlier assignment[12] to 803 cm^{-1}. The NN stretching mode is about 200 wavenumbers lower in the gas phase than in the solid, indicative of dative bonding between SbF_6^- and the terminal diazo nitrogen in the solid.

Energetics and Thermochemistry. *Model Dependency of Relative Energies.* The model dependencies of the energies of the b- and c-type structures relative to the open isomers are shown in Figure 5. Relative energies are shown in each case for 12 theoretical models. The first six theoretical models are based on

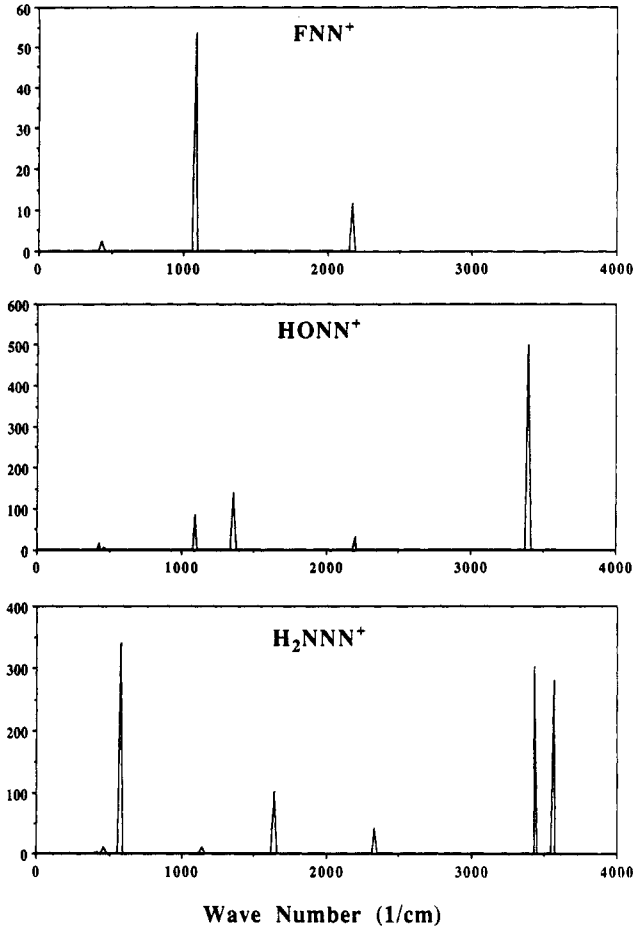

Figure 4. Computed infrared spectra of the open isomers of fluoro- (**1a**), hydroxy- (**2a**), and aminodiazonium ions (**3a**) as determined at the MP2(full)/6-31G* level.

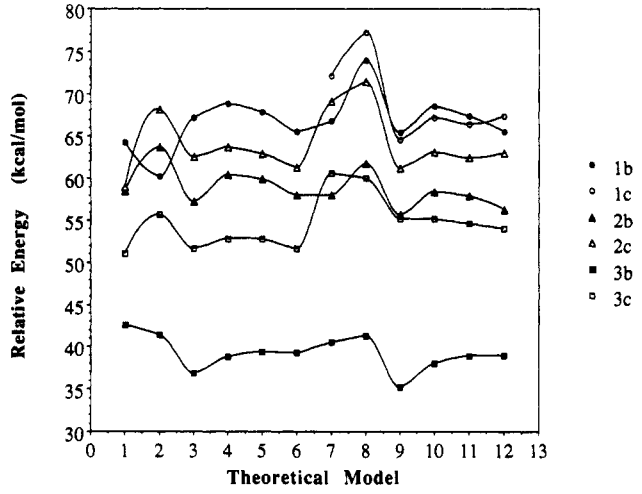

Figure 5. Energies of the symmetrically bridged b-type structures (solid marks) and of the c-type transition state structures (unfilled marks) relativd to the classical open isomers in kilocalories per mole. Relative energies are shown in each case for 12 theoretical models with interpolation. See text for definition of the theoretical models.

the RHF/6-31G* geometries, and the subsequent six entries are based on the MP2(full)/6-31G* geometries. In each of these sets, the first entry refers to the relative energy at the level of optimization; that is, models 1 and 7 are RHF/6-31G* and MP2-(full)/6-31G*. The models 2–6 and 8–12 refer to energy calculations with the MP2, MP3, MP4[DQ], MP4[SDQ], and MP4[SDTQ] methods and with the 6-31G** basis set in this order.

A few general comments are in order. (i) In going from the RHF level to the MP2 level relative energies change dramatically,

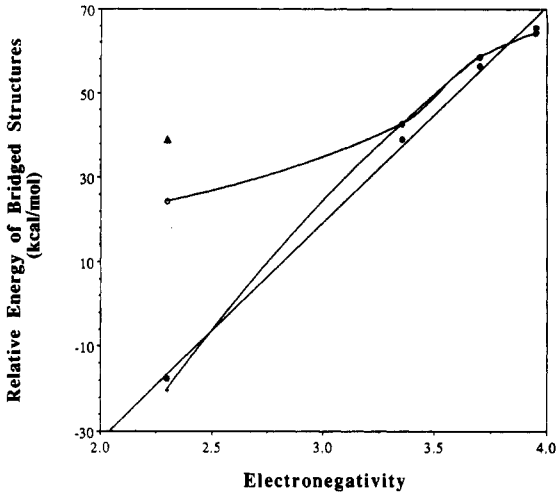

Figure 6. Energies of the symmetrically bridged structures of **1–3** relative to the open isomers in kilocalories per mole as determined at the MP4-[SDTQ]/6-311G**//MP2(full)/6-31G* (filled marks) and the RHF/6-31G* (unfilled marks) levels. Two interpolation lines are drawn at the RHF level depending on whether methyldiazonium ion (unfilled circles) or $CHNN^+$ (+ signs) was used. The regression line for the correlated energies includes the energy for $CHNN^+$ while that for methyldiazonium ion (triangle) is omitted.

and these changes can be as large as 9 kcal/mol (**2c**) although they are usually less than 5 kcal/mol. More importantly, the often held opinion that electron correlation would favor bridged structures over open structures holds in our case only for **1b** and **3b** but **2b**, **2c**, and **3c** become relatively less stable. (ii) The changes to the relative energies in going from second- to third-order corrections generally are in the opposite direction than those associated with going from model 1 to model 2. But again, there are exceptions such as **3b**. (iii) Fourth-order corrections at the MP4[DQ] level in all cases stabilize the open isomer more than the bridged species compared to the third-order treatment. The subsequent inclusion of single and triple excitation either has no effect (**3b**) or, more usually, leads to a relative destabilization of the open isomer (models 4–6), or it may affect the relative energies in the opposite direction (models 10–12 for **3b**). (iv) The changes to the relative energies also are quite sensitive to the structures as can be seen from the pairs of the models 2 and 3 versus the models 8 and 9. There are some trends in the dependency of the relative energies on the theoretical model but *none* of them is general, and this fact needs to be kept in mind in the interpretation of the data. In the following, we will discuss our highest level energies obtained at the MP4[SDTQ]/6-311G**//MP2(full)/6-31G* level. These energies probably are accurate to within 5 kcal/mol, an accuracy that certainly suffices to support our conclusions. Comparison with the RHF/6-31G* level is made as well.

Open versus Ring Structures. In Figure 6, the energies of the bridged b-structures relative to the open isomers are plotted versus the electronegativities of X. The interpolation line for the relative energies of **1–3** and methyldiazonium ion obtained at the RHF level (unfilled circles) shows that the preference for the open structure increases with the electronegativity of X in XNN^+ and, more importantly, that this relation is not a linear one. Clearly, electronegativity is only one factor that affects the relative stabilities of the a- and b-type structures. Aside from electronegativity differences, the number of lone pairs on the heterosubstituent X varies in the series of diazonium ion, and this may affect the relative stabilities. Since at least one of these lone pairs is crucial for the ring formation, methyldiazonium ion might not be the best carbon-substituted diazonium ion to compare with the hetero-systems **1–3**. We have therefore also considered the model system $HCNN^+$, a diazonium carbene ($^1A'$), as the CH group provides for a carbon substituent with a σ lone pair. Three stationary structures of the diazonium carbene (**4**) were localized at the RHF/6-31G* and at the MP2(full)/6-31G* levels (Tables I and II). The MP2 geometries are depicted in Figure 7 together with

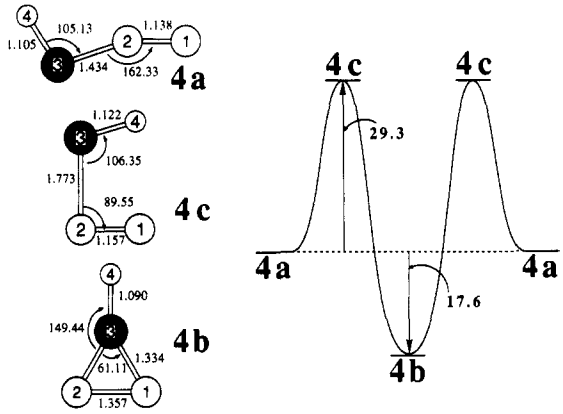

Figure 7. Reaction coordinate for the isomerization of diazonium carbene, $HCNN^+$. The open and the symmetrically bridged structures **4a** and **4b** are minima, and the nonclassical structure is the more stable one. Isomerization proceeds via the C_s structure **4c**. The structures shown were obtained at the MP2(full)/6-31G* level, and the energies were determined at the MP4[SDTQ]/6-311G**//RHF/6-31G* level. The relative energy between **4a** and **4b** at that level but based on the MP2 structures is only slightly different (17.7 kcal/mol).

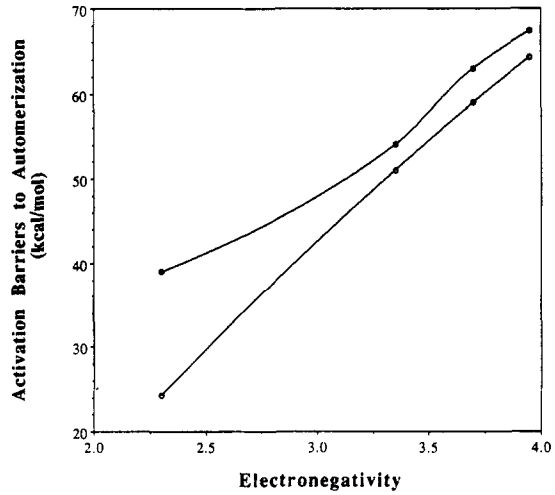

Figure 8. Activation barriers for automerization as determined at the levels MP4[SDTQ]/6-311G*//MP2(full)/6-31G* (filled marks) and RHF/6-31G* (unfilled marks) in kilocalories per mole.

a schematic drawing of the potential energy surface. As with **1–3**, both the open and the symmetrically bridged structures are minima, but the ring structure is the most stable isomer of **4**. If **4** is used instead of methyldiazonium ion in the plot of the relative energy of the ring systems versus the electronegativity (Figure 6, + marks), a nearly straight interpolation line is obtained. For the corresponding plot with the MP4[SDTQ]/6-311G**//MP2(full)/6-31G* relative energies (solid circles in Figure 6), we have in fact drawn a regression line instead of an interpolation line, and the correlation[30] is better than one might have reason to expect. The value for the methyldiazonium ion is way above this regression line (solid triangle) as it lacks an electron pair for the formation of the ring structure. The open structures of **1–3** and of methyldiazonium ion are favored over the cyclic systems at all levels. At our highest level, the relative stabilities of the bridged structures are 65.5 (F), 56.3 (HO), 38.9 (NH_2), and 40.0 kcal/mol (CH_3) in the vibrationless state at absolute zero. With inclusion of the vibrational zero-point energies we obtain the values 64.0 (F), 55.9 (OH), 38.7 (NH_2), and 36.9 kcal/mol (CH_3).

Activation Energies for Automerization. The activation barriers for the automerization processes of methyldiazonium ion and its heteroderivatives **1–3** are plotted versus the electronegativity of X in Figure 8. Correlation effects generally increase the activation

(30) Relative energy = −134.71 + 51.276 × electronegativity, with R^2 = 0.997.

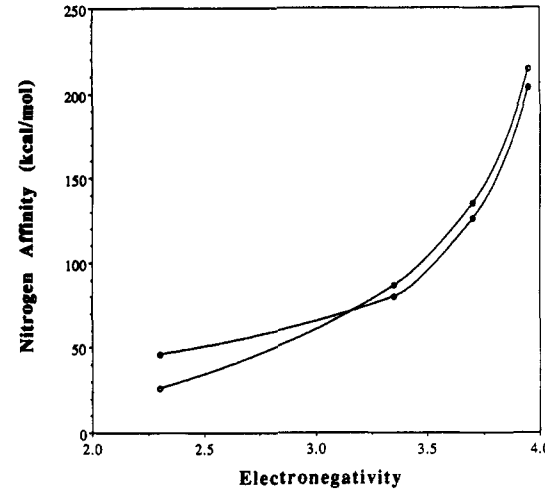

Figure 9. Plot of the dediazoniation energies versus the electronegativities. Values obtained at the MP4[SDTQ]/6-311G*//MP2(full)/6-31G* are shown as solid circles, and the unfilled circles correspond to the RHF/6-31G* values.

barriers by about 5 kcal/mol and more for the methyldiazonium ion. In contrast to the methyldiazonium ion, **1–3** are predicted to be kinetically stable toward N scrambling at ambient temperatures.

X^+ Cation Nitrogen Affinities. All of the heterosubstituted diazonium ions are thermodynamically stable with regard to dediazoniation. The loss of dinitrogen is endothermic in all cases. In Figure 9, the nitrogen affinities—the negative reaction energies of the dediazoniation reactions—are plotted versus the electronegativity of the X group. The bond strength of the X–N_2 linkage greatly increases with the X electronegativity. At the highest level employed here, the nitrogen affinities are 203.8 (F), 125.9 (OH), 79.7 (NH_2), and 45.9 kcal/mol[31] (CH_3). The nitrogen affinity of methyl cation allows for facile nucleophilic substitution reactions of methyldiazonium ion. McGarrity and Cox[32] succeeded in generating methyldiazonium ion by protonation of diazomethane in superacid media (HSO_4F, SO_2ClF, −120 °C), and they found that methyldiazonium ion decomposes even at low temperatures (−85 °C) under those conditions. In contrast to methyldiazonium ion, nucleophilic substitution at the amino nitrogen of **3** would require significant activation energy and proceed via an S_N2 path, and for **1** and **2** S_N chemistry seems unlikely. This result agrees well with recent experimental results by Olah et al. that conclusively showed that FNN^+ is unable to serve as an F^+ source.[33]

Diazonium Ion Acidity: Gas-Phase Proton Affinities. To determine the thermodynamic stability of **2**, **3**, and methyldiazonium ion with regard to deprotonation, we have considered the molecules N_2O, hydrazoic acid,[34] HN_3, and diazomethane, (CH_2N_2). The MP2(full)/6-31G* optimized geometries are summarized in Table III together with the RHF/6-31G* parameters reported by Kahn, Hehre, and Pople[35] and with the experimentally determined geometries. Although contributions of diradical character have been discussed for such 1,3-dipoles, Kahn et al. found that UHF wave functions collapse to the RHF solution in all of these cases. The structures were taken to be linear (N_2O), planar (HN_3), or C_{2v} symmetric (CH_2N_2). Frequencies were then computed to confirm that minima were indeed located, and in doing so, we found, surprisingly, that the C_{2v} symmetric structure of diazomethane is *not* a minimum at the correlated level. C_{2v} diazomethane

(31) For higher level studies of the methyl cation affinity, see ref 8.

(32) McGarrity, J. F.; Cox, D. P. *J. Am. Chem. Soc.* **1983**, *105*, 3961.

(33) Olah, G. A.; Laali, K.; Farnia, M.; Shih, J.; Singh, B. S.; Schach, C. J.; Christe, K. O. *J. Org. Chem.* **1985**, *50*, 1338.

(34) For recent theoretical work on HN_3 and a summary of prior results, see: Alexander, M. H.; Werner, H.-J.; Dagdigan, P. J. *J. Chem. Phys.* **1988**, *89*, 1388. Our best energies are considerably lower than the energies reported there.

(35) Kahn, S. D.; Hehre, W. J.; Pople, J. A. *J. Am. Chem. Soc.* **1987**, *109*, 1871.

exhibits one imaginary frequency (i94 cm^{-1}, b_1), and the associated displacement vector indicates a CH_2 pyramidalization motion leading to a C_s structure. The C_s minimum of diazomethane was located on the MP2 potential energy surface. In the resulting structure, the bond lengths are the same as in the C_{2v} structure and only angles are changed. Most notably, the CH_2 group shows a slight pyramidalization—the dihedral angle between the HCN and the symmetry planes is 94.9°—and the CNN backbone deviates a modest 1.2° from linearity. The potential energy is not affected much at all; the C_s structure is preferred by less than 10 cal/mol over the C_{2v} symmetric structure.[36] While the possibility of C_s symmetry for CH_2N_2 is intriguing and deserves further study at higher levels, our data is important in that it shows that small CH_2 pyramidalization *does not increase* the energy significantly. This is contrary to expectations based on the assumption that the CN bond has a strong π-bond component.

The computed structures of N_2O, HN_3, and CH_2N_2 are in reasonable agreement with the experimental geometries, and the deviations are generally larger for the N–N bonds than for the X–N bonds. The Δ(N–N) and Δ(X–N) values given in Table III show that the RHF computations generally underestimate and the MP2 computations overestimate the bond lengths. Both the N–N and the X–N bonds are rather short in all cases, and Kahn et al.[35] as well as Cooper et al.[37] suggested to describe these molecules as *hypervalent structures* to appropriately reflect the structural indication of both X–N double-bond and N–N triple-bond character.

The structural effects of protonation of diazomethane are as expected. At the correlated level, we find a typical increase of the CN bond length of 0.150 Å. The NN bond length is affected very little, and moreover it shortens by 0.022 Å; that is, the N_2 group in the diazonium ion structurally resembles molecular nitrogen more. Similar shortenings of the NN bond length also are found for N_2O (0.031 Å) and HN_3 (0.022 Å). But for N_2O and HN_3 protonation has surprisingly little effect on the X–N bond lengths as they lengthen only slightly by 0.079 and 0.050 Å.

Absolute proton affinities vary considerably over a range of about 20 kcal/mol (Table I), and relative affinities may still vary as much as 10 kcal/mol. At the highest level, proton affinities of 140, 189, and 226 kcal/mol are found for N_2O, HN_3, and CH_2N_2, respectively. The consideration of the vibrational zero-point energies reduces these values to 134, 181, and 217 kcal/mol. The proton affinities increase as the X electronegativity decreases. Bohme, Mackay, and Schiff[38] measured the proton affinity of N_2O and found a value of 137 (3) kcal/mol. Our theoretical value is in reasonable agreement with their result. The proton affinities of N_2O and of HN_3 may be compared to the experimentally determined gas-phase proton affinities[39] of 167 and 206 kcal/mol of H_2O and NH_3. The proton affinities of N_2O and of HN_3 are lower by about 33 and 25 kcal/mol, respectively, and they indicate that the double-bond character of the O–N bond in N_2O is reduced less than the one of the HN–N_2 bond in hydrazoic acid upon protonation. Finally, the relative proton affinities can be converted into relative pK_a differences. Under consideration of appropriate error bars for the affinities, we find that hydroxydiazonium ion is more acidic than aminodiazonium ion by ΔpK_a = 1.69 (6) and that the latter is more acidic than methyldiazonium ion by ΔpK_a = 1.56 (6).

Stereochemistry of the Ring-Opening Reactions. Structure I shows the generic Lewis structure for systems of the b-type. This structure implies that bonding between X and the basal N_2 fragment is achieved via two (localized) bonds, and in the LCAO method, these bonds correspond to the two delocalized MOs II and III. MO II involves a bonding interaction between the

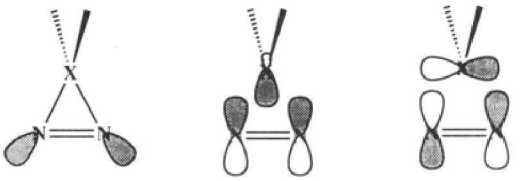

I II III

in-plane π-type orbital of N_2 and an a-symmetric sp^2 hybrid orbital of X. MO III is b-symmetric and results from bonding overlap between a p-type orbital of X with the in-plane π^* N_2 group orbital. If we look at the ring formation as the approach of X^+ to neutral N_2, II and III would mediate the electron donation toward and back-donation from X. The geometries of the b-type structures and the X^+ affinities of N_2 together with the relative stabilities of the a- and b-type structures show that these combined bonding interactions increase with the electronegativity of X, but to determine their individual importance—that is, to determine the electron density distribution in the ring—further information is required. This additional information may either come (a) indirectly from the comparative analysis of additional structures or (b) directly from an analysis of the electron density function. This information is necessary to understand the stereochemistry of the ring-opening reaction.

The examination of the transition-state structures for automerization is the obvious choice in following alternative (a). The structural differences between the b- and the c-type structures perturb the interactions to a different degree, and the energetic cost of these perturbations allows one to qualitatively estimate the contributions of II and III using basic orbital correlation

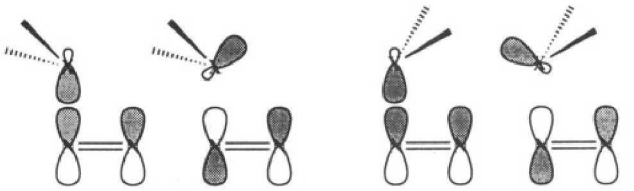

II III II III

"endo" "exo"

concepts. As we slide X parallel to N_2, II will become slightly less bonding for overlap reasons and because the hybridization of the X orbital would have to increase its p-character while III would become quickly nonbonding as the p-type X orbital has to become a lone pair. Thus, if the interaction III were important for ring formation, then we would expect a large increase in energy as X moves away from the symmetrically bridging position, and vice versa. Considering the relative energies of the b- and the c-type structures of **1–3**, we would conlcude that the ring formation of the fluoro system is due mainly to interaction II and that the interaction III becomes increasingly important for **2** and **3**. This MO theoretical result is in fact borne out by the analysis of the electron density functions (vide infra). This perturbation analysis points up that the p-type X orbital needs to become a lone pair, and there are consequences for the stereochemistry of the transition states. The lone pair can in principle develop in either one of two directions, leading to structures in which the developing X lone pair either is oriented toward the disconnected N ("endo") or away from it ("exo"). From the transition-state structures, we know that the "exo" fashion of the ring opening actually occurs (compare **3c**). This finding might be interpreted by invocation of minimization of electron–electron repulsion between the developing lone pair and the forming NN triple bond. If we had used the generic Lewis structure I as a representation of the bonding, we

(36) The consideration of the vibrational zero-point energies computed at the MP2 level would seem to suggest that the C_{2v} structure actually is preferred. Note, however, that all vibrational frequencies except for the lowest one are essentially the same for C_s and C_{2v} diazomethane and that the ΔVZPE merely reflects difference in the lowest frequency.

(37) Cooper, D. L.; Gerratt, J.; Raimondi, M. *J. Chem. Soc., Perkin Trans. 2* **1989**, 1187.

(38) Bohme, D. K.; Mackay, G. I.; Schiff, H. I. *J. Chem. Phys.* **1980**, *73*, 4976.

(39) Water: Collyer, S. M.; McMahon, T. B. *J. Phys. Chem.* **1983**, *87*, 909. Ammonia: Jenkins, H. D. B.; Morris, D. F. C. *J. Chem. Soc., Faraday Trans. 2* **1984**, *80*, 1167.

TABLE V: Topological Properties of the Ring Structures[a]

	A	B	r_A	r_B	F	ρ	λ_1	λ_2	λ_3	ϵ
					(FNN)$^+$, Bridged, **1b**					
					RHF/6-31G*//RHF/6-31G*					
1[b]	F3	N1	0.810	0.876	0.480	0.198	−0.389	−0.085	0.944	3.547
2	N1	N2	0.568	0.568	0.500	0.653	−1.990	−1.438	0.910	0.384
					MP2(full)/6-31G*//MP2(full)/6-31G*					
1[b]	F3	N1	0.827	0.790	0.511	0.174	−0.333	−0.052	0.940	5.350
2	N1	N2	0.604	0.604	0.500	0.542	−1.551	−1.163	1.158	0.333
R	F3	N1	0.822	0.889	0.481	0.173	−0.329	0.028	0.951	
					(HONN)$^+$, Bridged, **2b**					
					RHF/6-31G*//RHF/6-31G*					
1	O3	H4	0.813	0.166	0.831	0.326	−1.935	−1.887	1.635	0.026
2[b]	O3	N1	0.797	0.931	0.461	0.181	−0.349	−0.035	0.704	8.831
3	N2	N1	0.562	0.562	0.500	0.614	−1.898	−1.488	0.860	0.275
					MP2(full)/6-31G*//MP2(full)/6-31G*					
1	O3	H4	0.828	0.183	0.819	0.295	−1.562	−1.537	1.484	0.016
2[b]	O3	N1	0.820	0.761	0.518	0.197	−0.395	−0.148	0.823	1.677
3	N2	N1	0.607	0.607	0.500	0.530	−1.446	−1.133	1.137	0.277
R	O3	N1	0.813	0.885	0.479	0.192	−0.373	0.088	0.819	
					(H_2NNN)$^+$, Bridged, **3b**					
					RHF/6-31G*//RHF/6-31G*					
1[c]	N3	N1	0.738	0.728	0.503	0.277	−0.591	−0.227	0.660	1.606
2	N3	H4	0.797	0.211	0.791	0.332	−1.477	−1.437	1.116	0.028
3	N2	N1	0.581	0.581	0.500	0.605	−1.671	−1.314	0.926	0.272
R	N3	N1	0.852	0.723	0.541	0.568	−0.545	0.134	0.666	
					MP2(full)/6-31G*//MP2(full)/6-31G*					
1[c]	N3	N1	0.755	0.739	0.505	0.255	−0.535	−0.289	0.719	0.849
2	N3	H4	0.808	0.219	0.787	0.310	−1.322	−1.292	1.019	0.023
3	N2	N1	0.618	0.618	0.500	0.496	−1.266	−1.037	1.107	0.220
R	N3	N1	0.762	0.859	0.470	0.238	−0.469	0.192	0.662	
					(CHNN)$^+$, Bridged, **4b**					
					RHF/6-31G*//RHF/6-31G*					
1	N1	N2	0.643	0.643	0.500	0.446	−1.005	−0.826	0.894	0.218
2[c]	N1	C3	0.869	0.437	0.666	0.375	−0.912	−0.659	0.837	0.383
3	C3	H4	0.776	0.302	0.720	0.288	−0.928	−0.917	0.461	0.012
R	N1	C3	0.840	0.585	0.569	0.332	−0.556	0.190	0.565	

[a] The values r_A and r_B are the distances of the critical point (CP) from atoms A and B (in Å), F is the ratio $r_A/(r_A + r_B)$, ρ is the value of the electron density at the CP (in e au^{-3}, the λ_i are the principal curvatures of ρ at the CP, and the bond ellipticity is derived via $\epsilon = \lambda_n/\lambda_m - 1$, where $\lambda_n < \lambda_m$ and $\lambda_i < 0$. [b] For T-shaped molecular graphs the X–N1 and X–N2 bond critical points merge. [c] Only one of the symmetrically related X–N1 and X–N2 bond critical points is given.

would have had to conclude that the stereochemistry of the ring opening would follow the "endo" path. The representation I implies that there are two X–N bonds each involving one (approximately) sp^3 hybridized X orbital, and note especially, it implies *equal* importance of the interactions II and III. To corroborate the MO theoretical result that III is much less important than II, we have analyzed the electron density functions of **1b–3b** directly.

Surface plots of the cross sections of the MP2(full)/6-31G* electron density distributions in the ring plane are shown in Figure 10 for **1b–3b**. These plots impressively demonstrate that electron density accumulation occurs primarily in the centers of the ring and along the line between the midpoint of the N_2 group and X but *not* along the two "N–X bonds". The dominance of the type II interactions is clearly manifested in all cases. In Table V, the topological properties of the RHF/6-31G* and of the MP2-(full)/6-31G* electron density distributions are summarized and with these values the molecular graphs of the ring structures can be described in more quantitative terms. At the correlated level, all of the structures of **1b–3b** formally exhibit a ring critical point, but the differences between the values of the electron density at the ring critical points and at the adjacent N–X bond critical points are essentially null (0.001 for **1b**) or very small (0.005 for **2b** and 0.017 for **3b**). The molecular graph[40] of **1b** essentially is T-shaped, and the ring graphs of **2b** and **3c** resemble it closely. The curvature of the electron density of **1b** taken at the X–N bond critical point, perpendicular to the bond path, and in the molecular plane ($\lambda_2 = -0.052$) and the corresponding value at the ring critical point ($\lambda_2 = 0.028$) both are very small. The fact that the molecular graph of **1b** closely resembles a T-shaped one also is borne out in the extremely large value of the ellipticity of the N–X bond critical point ($\epsilon = 5.350$). The corresponding curvatures of the amino derivative **3b** are −0.289 and 0.192 at the bond and ring critical points, respectively, and the N–NH_2 ellipticity is $\epsilon = 0.849$. These critical points are still in close proximity of each other, and the molecular graph is extremely concave reflecting the dominance of the type II interaction. The values of the electron density at the N–X critical points are 0.174 (**1b**), 0.197 (**2b**), and 0.255 (**3b**). These values increase as the electronegativity of X decreases, and more importantly, they increase as the binding energy between X^+ and N_2 *decreases* for the bridged structures (138.26 for **1b**, 69.55 for **2b**, and 40.74 kcal/mol for **3b** at the highest level). The magnitude of the electron density at the bond critical points is no indicator of bond strength.

The effects of electron correlation on the electron density distributions can be examined either by comparison of the corresponding topological values determined at the RHF/6-31G* and at the MP2(full)/6-31G* levels (Table IV), or much more conveniently, this information can be envisioned via plots of the electron density difference function $\Delta\rho = \rho(\text{MP2}) - \rho(\text{RHF})$. These functions are shown in Figure 11 for **1b** and **3b**. For the N_2 fragment, the major effects of electron correlation can be

(40) For a discussion of concave- and convex-shaped molecular graphs in three-membered rings, see also: Cremer, D.; Kraka, E. *J. Am. Chem. Soc.* **1985**, *107*, 3800.

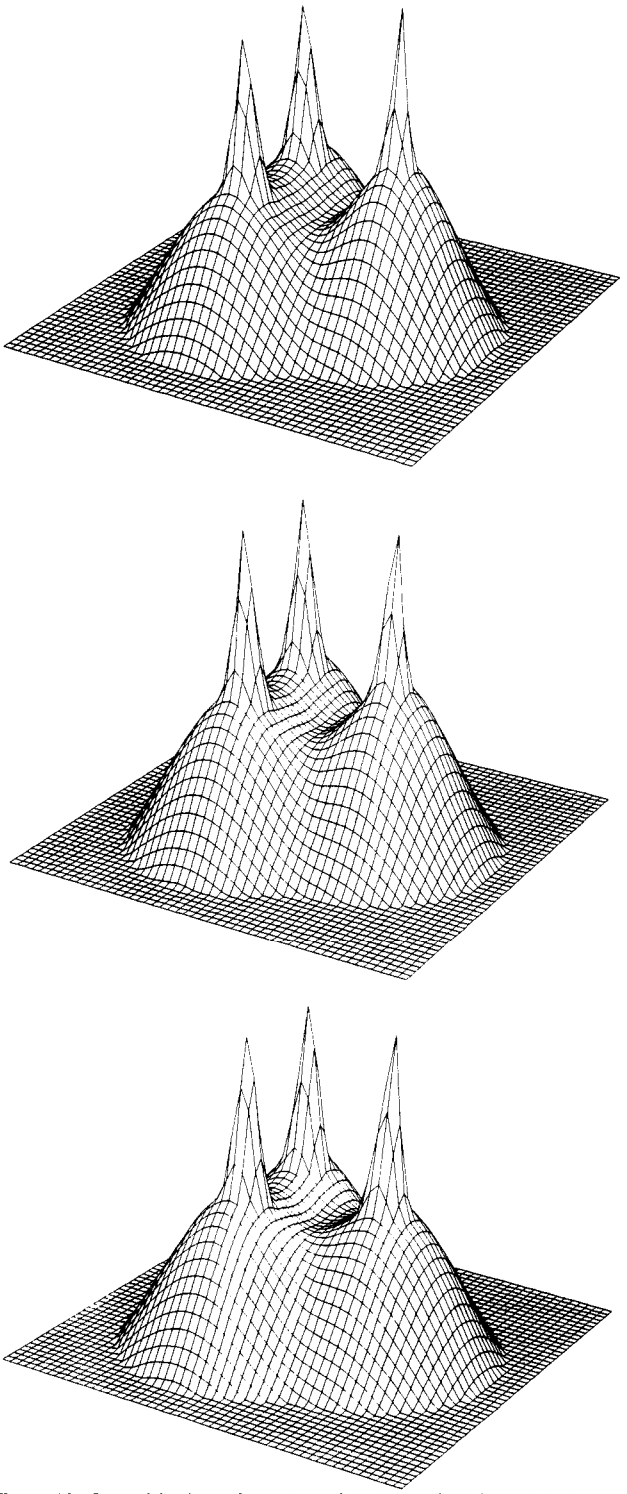

Figure 10. Logarithmic surface plots of the MP2(full)/6-31G* electron density distributions in the ring planes of (top to bottom) fluoro- (**1b**), hydroxy- (**2b**), and aminodiazonium ions (**3b**).

described as significant increases of the electron density in the in-plane π orbital regions and decreases in the N_2 σ group orbital regions. As to the electron density at X, electron correlation causes an accumulation of electron density in the σ orbital that is directed toward the center of the ring and a depletion of electron density in the region of the perpendicular in-plane p-orbital of X. An important difference between **1b** and **3b** relates to the magnitudes of the latter; electron correlation affects the more electronegative element more strongly (as expected). In all cases, electron correlation causes a reduction of electron density in the center of the ring as electron density is shifted more into the proximity of the atoms. As this reduction is larger in the ring center than along the N–X axes, electron correlation generally tends to change

TABLE VI

bridged diazonium ion	energetic stability		molecular graph	
	RHF	MP2	RHF	MP2
$(FNN)^+$	no	yes	T-shape	"T-shape"
$(HONN)^+$	yes	yes	T-shape	ring
$(H_2NNN)^+$	yes	yes	ring	ring
$(H_3CNN)^+$	no	no	"T-shape"	T-shape

T-shaped molecular graphs into ring graphs or, similarly, to make ring graphs less concave. Increased importance of the type III interactions at the correlated level might reasonably well have been anticipated as the origin of the changes to the molecular graphs, but the electron densities argue against this expectation. We note that the tendency toward the formation of a (or of a more stable) ring molecular graph from a T-shaped (or an extremely concave) graph parallels the kinetic stability of the symmetrically bridged structures (Table VI). But it needs to be said at the same time that the relation between the molecular graph and the kinetic stability of the molecule is not general. While kinetically unstable molecules do have T-shaped graphs, T-shaped graphs may also be found for the electron densities of molecules that are kinetically quite stable. **1b** and **2b** are examples and **2b** is an especially good one.

Summary and Conclusion

At the correlated level, the ring structures **1b–3b** are local minima and intermediates in the two-step automerizations of the more stable open structures **1a–3a**. The IR spectrum of **1a** agrees well with the one calculated at the correlated level, and the reassignment of the deformational mode is confirmed. Electron correlation affects the potential energy surfaces of **1** and **3** in a *qualitative* manner. At the RHF/6-31G* level, **1b** is not a local minimum but the automerization transition-state structure. This result points up that deductions regarding the activation barrier of automerization of **1** that are based on the RHF structures—even if higher level energies were calculated—are erroneous regarding the *mode* of automerization and its associated *activation barriers*. A more subtle qualitative difference relates to the automerization of **3**. C_s symmetry is maintained during isomerization on the RHF surface, but at the correlated level it involves enantiomerically related pathways with chiral transition-state structures in which the NH_2 group is twisted most likely to minimize lone-pair repulsion. In contrast to an earlier RHF/3-21G study, we find the most stable minimum of **3** to have a pyramidal NH_2 group and overall C_s—not C_{2v}—symmetry. The C_{2v} structure is the transition-state structure for facile NH_2 inversion. This result suggests that H_2N–N π-bonding is less important than had previously been thought.

The preference for the open isomers of XNN^+ increases with the X electronegativity in a nonlinear fashion. The consideration of carbene diazonium ion as a model C-substituted diazonium ion suggests that the availability of a lone pair at X is another important factor aside from electronegativity. At our highest level, the isomer preference energies are 64.0 (F), 55.9 (OH), 38.7 (NH_2), and 36.9 kcal/mol (CH_3) and automerization of the open structures require 65.5 (F), 56.3 (OH), 50.0 (NH_2), and 40.0 kcal/mol (CH_3) activation. **1–3** are predicted to be kinetically stable toward N scrambling at ambient temperatures in contrast to **5**.

1a–3a are more stable toward dediazoniation than **5**. The bond strength of the X–N_2 linkage greatly increases with X electronegativity. The cation nitrogen affinities are 203.8 (F), 125.9 (OH), 79.7 (NH_2), and 45.9 kcal/mol (CH_3). While **5** shows S_N1 chemistry, S_N reactions at the NH_2 nitrogen of **3** require significant activation and proceed via an S_N2 path, and for **1** and **2** S_N chemistry seems unlikely.

The geometries and the dediazoniation energies of the rings show that the ring stabilities increase with X electronegativity. Basic concepts of orbital correlation, the molecular graphs, and topological properties show that the ring bonding is dominated by the a-symmetric interaction between X and N_2. This type of

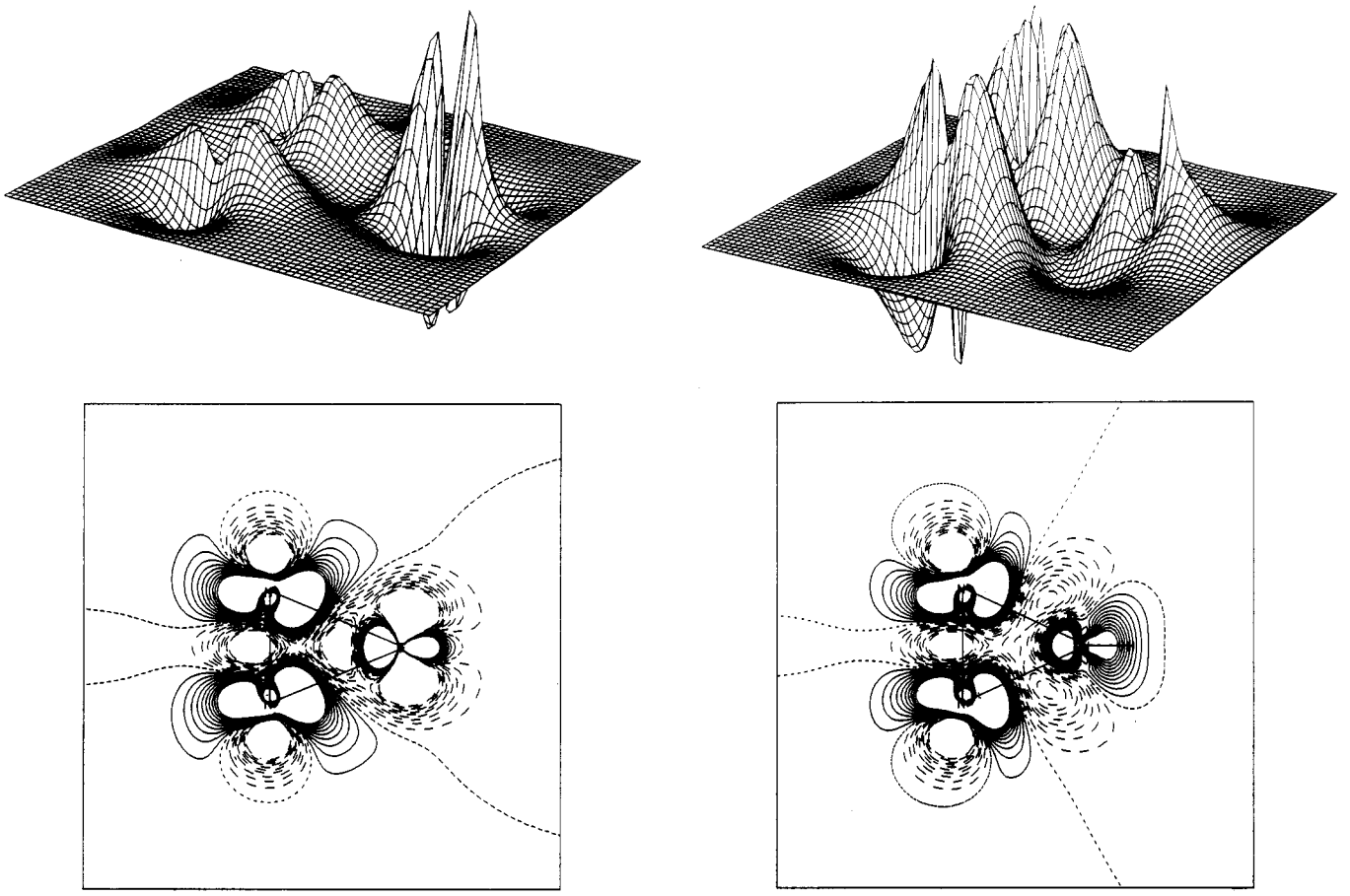

Figure 11. Surface and contour plots of the electron density difference function $\Delta\rho = \rho(\text{MP2}) - \rho(\text{RHF})$ of the symmetrically bridged structures of fluorodiazonium ion **1b** (left) and of aminodiazonium ion **3b**. Densities were determined with the 6-31G* basis set and with the MP2(full)/6-31G* geometries. Positive areas of $\Delta\rho$ are contoured with solid lines, short dash indicates $\Delta\rho = 0$, and long dashed lines are used to contour negative regions of $\Delta\rho$. Contours start at -0.01 e au^{-3}, and their value is increased in increments of 0.001.

bonding together with the MO theoretical perturbation analysis explains the "exo" stereochemistry of the ring-opening reaction while the generic Lewis ring structures would imply an "endo" stereochemistry. Moreover, the ρ values in the ring regions increase with decreasing X electronegativity and with decreasing binding energy between X^+ and N_2; that is, these ρ values are no indicator of bond strength. Graphical analysis of the functions $\Delta\rho = \rho(\text{MP2}) - \rho(\text{RHF})$ shows a general tendency of electron correlation to change T-shaped molecular graphs into ring graphs but not as the result of increased b-type interactions. While kinetically unstable ring structures do have T-shaped graphs, T-shaped graphs may also be found for kinetically quite stable molecules.

The computed structures and frequencies of N_2O, HN_3, and CH_2N_2 are in good agreement with experimental data. We found, surprisingly, that C_{2v} CH_2N_2 is *not* the minimum at the correlated level but the inversion transition-state structure of C_s CH_2N_2 with a slightly pyramidalized CH_2 group. While the bond lengths suggest a description of these molecules as hypervalent *structures*, this finding suggests a weaker CN π bond than has previously been thought and presents a challenge to the discussion of hypervalent *bonding* in these molecules. Proton affinities of 134 (N_2O), 181 (HN_3), and 217 kcal/mol (CH_2N_2) were determined, and they increase as the X electronegativity decreases. **2** is more acidic than **3** by $\Delta pK_a = 1.69$ (6), and **3** is more acidic than **5** by $\Delta pK_a = 1.56$ (6).

Thus, relative isomer stabilities of the aliphatic diazonium ions, their activation energies for isomerization, and the X^+ cation nitrogen affinities all increase with increasing X electronegativity while the proton affinities of the conjugated bases decrease with increasing X electronegativity. These results suggest that more stable alkyldiazonium ions might be accessible if the alkyl group is modified in such a way as to increase its overall electronegativity while keeping the concomitant acidity increase to a minimum.

Acknowledgment. This work was supported by a National Institutes of Health Institutional Biomedical Research Support Grant (No. RR 07053). We thank the Campus Computing Center for a generous allowance of computer time and Professor Schlemper for computer time on his Vaxstation3520. Acknowledgment is made to the donors of the Petroleum Research Fund, administered by the American Chemical Society, for partial support of this research.